Anal. Chem. **1998,** *70,* 3103−3113

Accelerated Articles

Laser Desorption−Membrane Introduction Mass Spectrometry

Manish H. Soni,† John H. Callahan, and Stephen W. McElvany*

Analytical Chemistry Section, Code 6113, U.S. Naval Research Laboratory, Washington, D.C. 20375

In this paper we describe the first use of laser desorption in conjunction with membrane introduction mass spectrometry (MIMS). In this technique, a low-powered carbon dioxide laser is used to irradiate the low-pressure (vacuum) side of a silicone membrane during a typical MIMS analysis of an aqueous solution. The absorption of laser energy results in direct membrane heating and rapid desorption of permeate molecules. This improves both the sensitivity and response times of MIMS when analyzing compounds having high molecular weight and low volatility. Two simple interfaces are described for performing laser desorption inside and outside the vacuum manifold of a GCQ ion trap mass spectrometer. Together with flow injection (FI) sample introduction, we demonstrate direct on-line monitoring of aqueous solutions of high boiling point (200−530 °C) polynuclear aromatic hydrocarbons such as naphthalene, anthracene, pyrene, benzo[*b*]fluoranthene, and indeno[123-*cd*]pyrene.

Membrane introduction mass spectrometry (MIMS) is a method for analyzing ultralow levels of volatile organic compounds directly from liquids (e.g., water or organic solvents), gases (e.g., air), or solids (e.g., soil) without preconcentration. It involves the use of a semipermeable membrane that acts as a chemical separator (or a sieve) by allowing analyte molecules to selectively permeate into a mass spectrometer where they are ionized, mass analyzed, and detected. A number of membrane interfaces have been developed[1−7] and used in diverse applications in the fields of on-line environmental[2,8−12] and biological monitoring.[13−16] The theory and applications of MIMS have been extensively reviewed.[2,5,17−26]

For air and water matrixes, the homogeneous silicone polymer poly(dimethylsiloxane) (PDMS) is the most commonly used membrane, primarily due to its high selectivity for a variety of analytes and its chemical and physical stability. For aqueous solutions, the permeation of analyte molecules across the silicone membrane is often referred to as pervaporation and involves a

† Visiting scientist from Department of Chemistry, Purdue University, West Lafayette, IN 47907.

(1) Bier, M. E.; Cooks, R. G. *Anal. Chem.* **1987**, *59*, 597.
(2) LaPack, M. A.; Tou, J. C.; Enke, C. G. *Anal. Chem.* **1990**, *62*, 1265.
(3) Lauritsen, F. R. *Int. J. Mass Spectrom. Ion Processes* **1990**, *95*, 259.
(4) Slivon, L. E.; Bauer, M. R.; Ho, J. S.; Budde, W. *Anal. Chem.* **1991**, *63*, 1335.
(5) Kuban, V. *Crit. Rev. Anal. Chem.* **1992**, *23*, 323.
(6) Dejarme, L. E.; Bauer, S. J.; Cooks, R. G.; Lauritsen, F. R.; Kotiaho, T.; Graf, T. *Rapid Commun. Mass Spectrom.* **1993**, *7*, 935.
(7) Yakovlev, B. S.; Talrose, V. L.; Fenselau, C. *Anal. Chem.* **1994**, *66*, 1704.
(8) Kotiaho, T.; Hayward, M. J.; Cooks, R. G. *Anal. Chem.* **1991**, *63*, 1794.
(9) Soni, M.; Bauer, S.; Amy, J.; Wong, P.; Cooks, R. G. *Anal. Chem.* **1995**, *67*, 1409.
(10) Cisper, M. E.; Gill, C. G.; Townsend, L.; Hemberger, P. H. *Anal. Chem.* **1995**, *67*, 1413.
(11) Virkki, V. T.; Ketola, R. A.; Ojala, M.; Kotiaho, T.; Komppa, V.; Grove, A.; Facchetti, S. *Anal. Chem.* **1995**, *67*, 1421.
(12) Gordon, S. M.; Callahan, P. J.; Kenny, D. V.; Pleil, J. D. *Rapid Commun. Mass Spectrom.* **1996**, *10*, 1038.
(13) Hayward, M. J.; Kotiaho, T.; Lister, A. K.; Cooks, R. G.; Austin, G. D.; Narayan, R.; Tsao, G. T. *Anal. Chem.* **1990**, *62*, 1798.
(14) Lauritsen, F. R.; Kotiaho, T.; Lloyd, D. *Biol. Mass Spectrom.* **1993**, *22*, 585.
(15) Lauritsen, F. R.; Gylling, S. *Anal. Chem.* **1995**, *67*, 1418.
(16) Johnson, R. C.; Srinivasan, N.; Cooks, R. G.; Schell, D. *Rapid Commun. Mass Spectrom.* **1997**, *11*, 363.
(17) Tsai, G. J.; Austin, G. D.; Syu, M. J.; Tsao, G. T.; Hayward, M. J.; Kotiaho, T.; Cooks, R. G. *Anal. Chem.* **1991**, *63*, 2460.
(18) Kotiaho, T.; Lauritsen, F. R.; Choudhry, T. K.; Cooks, R. G. *Anal. Chem.* **1991**, *63*, 875A.
(19) Beebe, K. R.; Blaser, W.; Bredeweg, R.; Chauvel, J.; Harner, R.; LaPack, M.; Leugers, A.; Martin, D.; Wright, L.; Yalvac, E. *Anal. Chem.* **1993**, *65*, 199R.
(20) Patrik, J. S.; Wong, P.; Xu, C.; Soni, M.; Kasturikrishnan, N.; Srinivasan, N.; Cooks, R. G. *Proc. Control Quality* **1995**, *7*, 117.
(21) Wong, P. S. H.; Cooks, R. G.; Cisper, M. E.; Hemberger, P. H. *Environ. Sci. Technol.* **1995**, *29*, 215A.
(22) Bauer, S. *Trends Anal. Chem.* **1995**, *14*, 202.
(23) Overney, F. L.; Enke, C. G. *J. Am. Soc. Mass Spectrom.* **1996**, *7*, 93.
(24) Kotiaho, T. *J. Mass Spectrom.* **1996**, *31*, 1.
(25) Lauritsen, F. R.; Kotiaho, T. *Rev. Anal. Chem.* **1996**, *15*, 237.
(26) Srinivasan, N.; Johnson, R. C.; Kasthurikrishnan, N.; Wong, P.; Cooks, R. G. *Anal. Chim. Acta* **1997**, *350*, 257.

S0003-2700(98)00436-3 Not subject to U.S. Copyright. Publ. 1998 Am. Chem. Soc.
Published on Web 06/20/1998

liquid-to-vapor phase change. It is described as consisting of three separate stages: (i) preferential absorption of analyte molecules into the high-pressure (solution) side of the membrane, (ii) diffusion of the analyte across the membrane, and (iii) evaporation (desorption) of the molecules from the vacuum side of the membrane into the mass spectrometer.[2,17,27] Fick's laws of diffusion have been used to define the permeation rate (F) as,[2,17]

$$F = \frac{A}{L} D C_s$$

where F is the flow or permeation rate (mol/s), A is the membrane surface area (cm^2), D is the diffusion coefficient (cm^2/s), C_s is the concentration of analyte in the solution, and L is the membrane thickness (cm). This relationship is defined for steady-state conditions wherein the sample is introduced continuously so that its concentration across the membrane and, hence, the permeation rate are constant with time. For flow injection (FI) conditions, i.e, when the sample is introduced as small-volume plugs, the concentration across the membrane and, therefore, the permeation rate (F) change with time. In either case, the absorption of the analyte molecules from the solution into the membrane (stage i) is compound dependent and assumed to be linear, while the desorption or vaporization (stage iii) of the analyte from the vacuum side of the membrane is assumed to be nonselective and rapid, such that $C_2 = 0$, where C_2 is the analyte concentration at the vacuum (or low-pressure) side of the membrane surface (mol/cm^3). Therefore, for a given compound, under fixed operating conditions, the concentration gradient between the two membrane surfaces (high pressure and low pressure) is the principal driving force for permeation. It determines the magnitude of the response, while the diffusion coefficient, D, controls the response time. D is determined by the molecular size (it decreases as molecular size increases) and membrane temperature (it increases with temperature). The response time is defined as the delay between the time at which the sample reaches the solution side of the membrane and observation of the signal. In general, the relationship between F and C_s is linear for a given compound over a wide dynamic range.[2,17,35]

MIMS performance is strongly dependent on the efficiency of the pervaporation process. When analytes have low molecular weights and high volatility (high desorption rates), such that $C_2 = 0$, permeation is rapid, and MIMS performance is excellent. But, when the analytes become larger and less volatile (semivolatile), like the polynuclear aromatic hydrocarbons (PAHs) in this study, permeation is slow and limited by the rate of desorption of the semivolatile molecules from the membrane surface. If the rate of desorption is so low that $C_2 > 0$, then the concentration gradient ($C_s - C_2$) and, hence, the magnitude (sensitivity) of the MIMS response will decrease. Since the desorption process controls the permeation rate, the dynamic range linearity will also be affected. The slow desorption will also extend the response time and significantly degrade the performance. In these arguments, it is assumed that the diffusion coefficient is independent of analyte concentration and its desorption rate. Thus, increasing the rate of desorption (ideally such that $C_2 = 0$) and also the diffusion coefficient by increasing the membrane temperature is necessary to improve pervaporation efficiency and to make MIMS a viable technique for analyzing high boiling (semivolatile) analytes.

Several research groups have focused on the analysis of semivolatile samples using MIMS. For example, Lauritsen et al. have demonstrated a trap-and-release MIMS experiment for analyzing semivolatile species in water.[28,29] In their method, the silicone membrane is placed directly in the ionization region of the mass spectrometer. The proximity to the hot electron impact (EI) filament provides additional heat to the membrane. As the membrane temperature rises, so does the permeation rate and, hence, the sensitivity. Using trap-and-release MIMS, the authors have analyzed compounds such as fluoranthene (bp 385 °C), phenanthrene (bp 340 °C), and pentachlorophenol (bp 310 °C) at low parts-per-billion (ppb) levels in water.[28,29] Conventionally, higher membrane temperature is achieved by continuously heating the solution that flows across the membrane, resulting in thermal equilibrium between the membrane, solution, and surroundings. However, for practical reasons (e.g., bubble formation), the aqueous solution can only be heated to 80−85 °C by this technique. This temperature may not be sufficient to efficiently desorb semivolatile analytes.

Cisper and Hemberger[30] have recently shown that ultrathin (0.5 μm) supported silicone membranes are capable of detecting ppb levels of semivolatile species including methyl salicylate (bp 222 °C) and naphthalene (bp 218 °C) from air and 2-chlorophenol (bp 175 °C) from water. Their approach exploits the inverse relationship between permeation rate and membrane thickness as shown in the equation above. Upon reducing the membrane thickness, the permeation rate increases, while the time spent by the species in the membrane decreases, resulting in rapid and sensitive analysis. However, thin membranes do not influence the desorption rate of the species. In addition, as the membrane thickness decreases, the permeation of the matrix (water) also increases, which may be detrimental to the mass spectrometer vacuum and performance. The low mechanical strength of thin membranes could also limit its use for extended periods.

The analyte absorption and diffusion is dependent upon the interactions between the polymer and the analyte;[2,17,27] hence, chemically modifying the membrane[31] or using other types of membranes[27,32,33] may improve performance by increasing the permeation rate of the semivolatile species. A limited number of studies have been conducted in this field, but none addresses the issue of enhancing desorption of semivolatile analytes from the membrane surface. In terms of increasing the flux of larger species, the microporous membranes seem most promising. Microporous membranes, unlike the homogeneous silicone membrane, have a rigid, voided structure with randomly distributed interconnected pores. The permeation mechanism is different from that of silicone membranes in that the transport of large semivolatile species is rapid and limited only by the pore size

(27) Huang, R. Y. M., Ed. *Pervaporation Membrane Separation Processes*; Elsevier: New York, 1991.

(28) Leth, M.; Lauritsen, F. R. *Rapid. Commun. Mass Spectrom.* **1995**, *9*, 591.
(29) Lauritsen, F. R.; Ketola, R. A. *Anal. Chem.* **1997**, *69*, 4917.
(30) Cisper, M. E.; Hemberger, P. H. *Rapid. Commun. Mass Spectrom.* **1997**, *11*, 1449.
(31) Xu, C.; Patrick, J. S.; Cooks, R. G. *Anal. Chem.* **1995**, *67*, 724.
(32) Maden, A. J.; Hayward, M. J. *Anal. Chem.* **1996**, *68*, 1805.
(33) Kasthurikrishnan, N.; Cooks, R. G.; Bauer, S. *Rapid Commun. Mass Spectrom.* **1996**, *10*, 751.

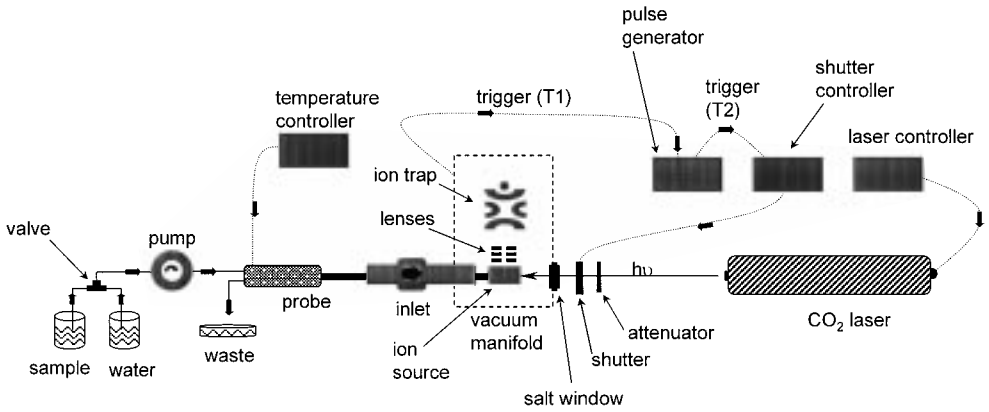

Figure 1. General experimental setup for LD−MIMS, showing the internal interface. In this configuration, laser desorption is carried out inside the GCQ vacuum manifold within the ionization region (ion source).

distribution. In practice, the high matrix (water) flux associated with porous membranes mandates the use of some means (e.g., a jet separator) to remove the excess water that permeates together with the analyte. This also makes them vacuum incompatible when used with direct insertion probes. Microporous membranes are also amenable to transport of polar species, as demonstrated by Wong and Cooks.[34] They used a microporous Teflon membrane to analyze polar species such as lactic acid (bp 122 °C) and 5-hydroxymethylfurfural (bp 116 °C) at ppb levels in aqueous solutions. In a separate study,[31] the same group used a chemically modified cellulose membrane to selectively monitor low parts-per-million (ppm) levels of benzaldehyde (bp 178 °C) from a complex aqueous mixture. In this method, called affinity MIMS, benzaldehyde molecules selectively bind to an alkylamine-modified cellulose membrane in the loading step (preconcentration) and are released via acid hydrolysis in the elution step. A unique feature of this method is the reversible nature of the reaction which allows highly specific continuous on-line monitoring. None of these methods, however, improves the rate of desorption of semivolatile species from the membrane surface.

In this paper we describe the first use of laser desorption to assist the analysis of semivolatile species using MIMS. In our method, referred to as laser desorption−membrane introduction mass spectrometry (LD−MIMS), a continuous wave (cw) carbon dioxide ($\lambda = 10.6\ \mu$m) laser is used to irradiate the vacuum side of a silicone membrane during analysis. This process deposits sufficient energy into the membrane surface to rapidly desorb intact neutral permeate molecules, which are then ionized using EI ionization and analyzed in an ion trap mass spectrometer. Two simple interfaces (internal and external) have been developed for use with a commercially available direct insertion sheet membrane probe (DIMP) and flow injection (FI) type sample introduction procedures. The technique allows us to demonstrate, for the first time, direct on-line monitoring of aqueous solutions of high boiling point polynuclear aromatic hydrocarbon (PAHs) including naphthalene (bp 218 °C), anthracene (bp 340 °C), pyrene (bp 393 °C), chrysene (bp 448 °C), benzo[*b*]fluoranthene (bp 480 °C), and indeno[123-*cd*]pyrene (bp 530 °C) by MIMS.

(34) Wong, P. S. H.; Cooks, R. G. *Anal. Chim. Acta* **1995**, *310*, 387.

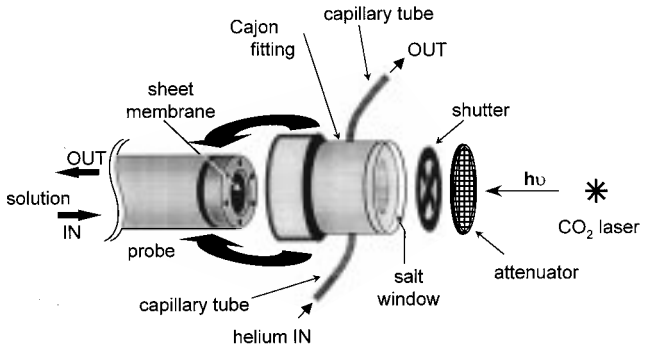

Figure 2. Schematic of the external LD−MIMS interface. See text for detailed description.

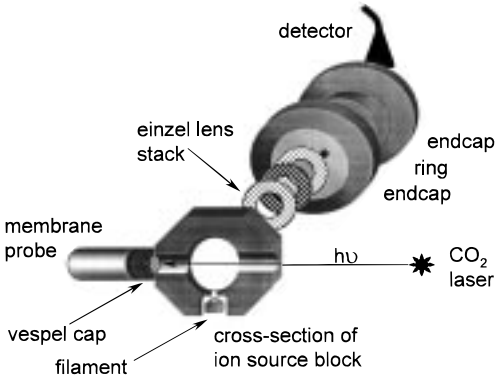

Figure 3. Schematic of the internal LD−MIMS interface. See text for detailed description.

EXPERIMENTAL SECTION

The general experimental setup used for LD−MIMS is shown in Figure 1 for the internal interface. Figures 2 and 3 show the external and internal interfaces in detail, respectively. All experiments were performed on a Finnigan GCQ ion trap mass spectrometer (Finnigan Corp., San Jose, CA) operated in the normal electron impact (EI) ionization and full scan (m/z 50−300) or selected ion monitoring (SIM) mode. The standard gas chromatograph was replaced with the MIMS interfaces, as described below. The instrument was operated using the standard Finnigan GCQ version 2.1 software and also Custom Tune (version 1.0 beta) instrument control software (Finnigan Corp., Austin, TX). Custom Tune allows users to build their own interface for operating the GCQ using the Visual Basic programming language

Table 1

GCQ parameter	value
temperature	ion source: 200,[a] 125[b] °C transfer line: 200,[a] na[b] °C
scan mode	full scan (first mass = 50, last mass = 300) SIM (SIM mass = variable, SIM width = 1.0)
ion injection rf	full scan mode auto mode[c] high mass adjust = 100% manual mode[d] first ion rf = 30−80 Da second ion rf = 30−80 Da injection time using second ion rf = 50% SIM scan mode auto mode[c] manual mode[d] ion rf level = 30−80 Da
ionization time	when AGC on ionization time = auto set[c] (target value = 50) when AGC off ionization time = manual set[d] (25−100 ms)
ionization mode	+ EI
emission current	300 μA
electron energy (on/off)	−70/−20 V
electron lens (on/off)	15/65 V
lens 1	−10 to −60 V
lens 3	−10 to −60 V
gate lens (on/off)	−90 to −100 V/100 V
trap offset	−10 to −20 V
electron multiplier	1200−1275 V
dynode	15 kV

[a] With external interface configuration. [b] With internal interface configuration. na, not applicable. [c] In auto mode, this parameter value is set automatically by the GCQ software. [d] In manual mode, this parameter value is manually set using the Custom Tune software.

(version 5.0, Microsoft's Visual Basic compiler, Microsoft Corp., Redmond, WA). We designed our Custom Tune interface to include manual control over such parameters as einzel lens voltages, EI source lens voltage, electron energy, emission current, ionization times, rf voltage levels, trap offset voltage, and automatic gain control (AGC). Additional displays were also programmed into Custom Tune to allow viewing of multiple-ion chromatograms (MIMS ion chromatograms are plots of ion intensities versus time or scan number) in real-time during acquisition. The GCQ is still autocalibrated and autotuned using standard procedures, but then the various parameters (listed above) are manually tuned (optimized) prior to each acquisition. Typical values used for these parameters and other ion trap conditions are tabulated in Table 1. All raw data (ion intensities versus scan number) were exported and processed using Microcal Origin version 4.1 statistical analysis program (Microcal Software Inc., Northampton, MA). Data processing included background subtraction, smoothing, and peak area and peak rise/fall time calculations.

A direct insertion membrane probe[1,22,35] (DIMP, MIMS Technology Inc., Palm Bay, FL) was used in both interfaces. The probe was fitted with a 0.010-in.-thick circular silicone sheet membrane (diameter 0.5 in., Dow Corning Corp., Midland, MI). Prior to mounting on the probe, the membrane was washed once with hexane and pure water and then vacuum-dried. The GCQ performance markedly degraded when a thinner (0.005 in.) membrane was used due to the high water influx. Hence, the thicker (0.010 in.) membrane had to be used for all experiments. In this probe design, the sheet membrane is sandwiched between a Teflon ring spacer on the solution side and a stainless steel cap on the vacuum side with six screws holding them together. This arrangement leaves a circular membrane area (0.2 in. diameter) exposed to the solution and vacuum. FI type sample introduction was employed, wherein 2−10-mL sample plugs were injected manually into a background stream of water that was continuously flowing through the probe using a three-way microtubing valve (catalog no. E-06473-15, Cole-Palmer Instrument Co., Vernon Hills, IL). The solution flow rate was optimized to 2 mL/min and maintained by a peristaltic pump (Anspec Co., Lincoln, NE). In experiments where a steady-state response was desired, the sample was introduced continuously. The DIMP was heated to 80 °C using the probe temperature controller[22,35] for all experiments (internal and external), unless otherwise indicated. In the external configuration, the GCQ transfer line and ion source were operated at 200 °C, while the interface in direct contact with the probe was heated to approximately the same temperature as the probe, viz. 80 °C. In the internal desorption experiment with the membrane in close proximity, the ion source has to be operated at a lower temperature of 125 °C to prevent membrane damage. Due to the heat radiated by the hot EI filament, the ion source temperature could not be lowered below 125 °C.

The CO_2 laser (model LS-55-ATVO, California Laser, San Marcos, CA) used is capable of a maximum continuous power output of 10 W at 10.6-μm wavelength. The laser controller, which also includes the power supply, and the laser itself are compact benchtop devices (laser dimensions 17.5 in. × 3.5 in. × 3.5 in.; controller dimensions 12 in. × 7 in. × 4 in.). An unfocused Gaussian laser beam having a spot size of approximately the same dimensions as the exposed membrane (0.2 in. diameter) was incident normal to the membrane surface. Irradiation was either continuous or pulsed. In the pulsed mode of operation, the cw beam was gated with a mechanical shutter (model SD-10 driver, Uniblitz shutter, Vincent Associates, Rochester, NY). The width and timing of the shutter were controlled by a TTL trigger pulse (T2) from a pulse generator (model DG535, S.R.S Inc., Sunnyvale, CA) which was synchronized to the start of the ionization period by an edge trigger (T1) from pin 18 of digital latch U68 on the main system PCB of the GCQ electronics. An important criterion in our experiment was that the fragile membrane had to be irradiated over multiple FI sampling periods of several minutes without being damaged. Therefore, the laser power was attenuated by almost an order of magnitude for both continuous and pulsed modes of operation. This was accomplished using a fine nickel mesh (10−75% transmission) to reduce the power density to <5 W/cm^2. When energies >5 W/cm^2 were used, even the defocused beam was capable of burning a hole in the membrane. In general, the membrane was replaced after about a total of 6 h of laser irradiation in these preliminary experiments.

Certified standards (20 μg/mL or ppm in methanol) of naphthalene (MW 128, bp 218 °C), anthracene (MW 178, bp 340

(35) Bauer, S.; Solyom, D. *Anal. Chem.* **1994**, *66*, 4422.

°C), pyrene (MW 202, bp 393 °C), chrysene (MW 228, 448 °C), benzo[*b*]fluoranthene (MW 252, bp 480 °C), and indeno[123-*cd*]-pyrene (MW 276, bp 530 °C) were obtained from Supelco Inc. (Bellefonte, PA) and diluted as needed using water obtained from a Millipore system (model Milli-Q+, Millipore Corp., Bedford, MA). This water also formed the background solution in the FI introduction.

External Interface. The external interface was used to perform laser desorption outside of the mass spectrometer (Figure 2). It was machined from a 0.5-in. Cajon adapter fitting (part no. SS8UTA12, Swagelok Co., Macedonia, OH). One end of the interface was sealed with an IR-transparent thallium bromoiodide salt window (KRS-5, 25 mm diameter, 4 mm thickness, Wilmad, Buena, NJ) using Torr-Seal. The membrane probe fits in the Cajon fitting through the open end to form a vacuum-tight seal. The inside of the interface was continuously flushed with helium gas introduced through a silicosteel capillary (i.d. 0.5 mm) tube fitted to the interface. The helium gas transports the permeate and desorbate into the ion source via another silicosteel capillary which runs through the GCQ transfer line into the source. The helium flow rate was approximately 1.5 mL/min and yielded a pressure reading of 80 mTorr (fore pressure) and 1.0×10^{-4} Torr (ion gauge pressure) in the GCQ.

Internal Interface. The internal interface (Figure 3) was used to perform laser desorption directly in the ionization region of the mass spectrometer. It was designed from simple modifications to the GCQ ion source block and the EI ion volume. The GC transfer line was replaced with the membrane probe inlet/vacuum lock (MIMS Technology Inc.). The inlet shaft is hollow and supports the probe in the vacuum (Figure 1). It terminates in a small constriction with a Maycor tip which fits in the ion source block.[22,35] This was replaced with a custom-machined open-ended hollow shaft so the probe could be inserted all the way to the ion source. The standard stainless steel cap which supports the membrane on the vacuum side was replaced by a similar cap made from Vespel (SP1-polyimide, Dupont, Wilmington, DE). The thermal and electrical insulating Vespel cap allows the probe to be in direct contact with the hot ion source without damaging the membrane. The hole in the stainless steel source block where the GC transfer line connects was widened to 0.2-in. diameter to match the dimensions of the membrane. There is another hole on the opposite side where the calibration gas/CI reagent gas tubing is connected. This was also widened to 0.2-in. diameter and the connecting tubing was removed. The corresponding holes in the EI ion volume were similarly widened. A thin metal O-ring was attached to the source block to support the probe and keep the membrane aligned with the source block hole. The second GCQ vacuum port, which is normally capped, was fitted with a KBr salt window using standard Cajon fittings. Figure 3 shows the cross section of the modified source block and the probe location. The membrane literally forms one wall of the ion source and is normal to the CO_2 laser. The GCQ EI filament is orthogonal to the laser beam. Under these conditions, the operating pressure was $\sim 6 \times 10^{-5}$ Torr (ion gauge) and 30 mTorr (fore pressure).

RESULTS AND DISCUSSION

Laser-Induced Thermal Desorption. Lasers are widely used in the desorption and ionization of thermally labile and/or involatile species in mass spectrometry. The desorption and ionization processes have been accomplished either in a single step or in two separate steps.[36−42] In the latter case, the two processes are spatially and temporally resolved and thus can be independently controlled and optimized. Ionization in this case is often referred to as postionization. While lasers are commonly used for postionization, electron impact (EI) ionization is simpler and, unlike lasers, it is universal, i.e., it ionizes all desorbed molecules with roughly equal sensitivity. EI postionization is particularly suited for LD−MIMS since it can cause ionization to occur over the entire desorption period (several milliseconds), which greatly exceeds typical laser pulse widths. Among various reported descriptions of laser desorption/postionization experiments, of particular interest here are those involving the application of infrared lasers for desorbing intact neutral molecules from surfaces. In this case, the IR absorbing substrate is rapidly heated upon irradiation and causes surface-bound neutrals to desorb without decomposition. For example, Dale et al. have applied CO_2 laser desorption−UV laser postionization for analyzing PAHs in soils[43] and cloudwater aerosol filtrates.[44] In a unique application, Zare et al. recently used UV−laser desorption/UV−laser postionization to analyze PAHs present in a Martian meteorite.[45] For thermally stable species, laser-induced thermal desorption can be accomplished using low-powered ($<10^4$ W/cm^2) IR lasers.[39,41,46−49] In such cases, the desorption process has been theoretically modeled and shown to be analogous to conventional thermal desorption or vaporization.[39,46,48,49]

The concept of laser-assisted desorption in MIMS was originally proposed by Cooks et al. in 1991.[50] This paper reports the first successful demonstration of laser-induced desorption with MIMS. PAHs are good test compounds for this study because they are both transparent at the CO_2 laser wavelength and relatively thermally stable. Their analysis by conventional MIMS is hampered by their large size and low volatility, as discussed previously. On the other hand, the silicone membrane is IR absorbing and moderately thermally stable up to ~250 °C.[2] Its IR transmission spectrum, recorded using a model Cygnus 100 Mattson FT-IR spectrometer (Mattson Instruments Inc., Madison,

(36) Hillenkamp F.; Karas, M.; Beavis, R. C.; Chait, B. T. *Anal. Chem*. **1991**, *63*, 1193.
(37) Chait, B. T.; Kent, S. B. *Science* **1992**, *257*, 1885.
(38) Cotter, R. J. *Anal. Chim. Acta* **1987**, *195*, 45.
(39) Conzemius, R. J.; Capellen, J. M. *Int. J. Mass Spectrom. Ion Phys*. **1980**, *34*, 197.
(40) Li, L.; Lubman, D. M. *Rev. Sci. Instrum*. **1988**, *59*, 557.
(41) Grotemeyer, J.; Schlag, E. W. *Acc. Chem. Res*. **1989**, *22*, 399.
(42) Zare, R. N.; Zenobi, R. In *Advances in Multiphoton Processes and Spectroscopy*; Lin, S. H. Ed.; World Scientific: River Edge, NJ, 1991.
(43) Dale, M. J.; Jones, A. C.; Pollard, S. J.; Langridge-Smith, P. R. R.; Rowley, A. G. *Environ. Sci. Technol*. **1993**, *27*, 1693.
(44) Dale, M. J.; Downs, K. F.; Wright, S. J.; Langridge-Smith, P. R. R.; Cape, J. N. *Environ. Pollut*. **1995**, *89*, 123.
(45) McKay, D. S.; Gibson, E. K.; Thomas-Keprta, K. L.; Vali, H.; Romanek, C. S.; Clemett, S. J.; Chillier, X. D. F.; Maechling, C. R.; Zare, R. N. *Science* **1996**, *273*, 924.
(46) Stoll, R.; Rollgen, F. W. *Org. Mass Spectrom*. **1979**, *14*, 642.
(47) Weyssenhoff, H.; Selzle, H. L.; Schlag, E. W. *Z. Naturforsch*. **1985**, *40A*, 674.
(48) Chuang, T. J. *J. Electron. Spectrosc. Relat. Phenom*. **1983**, *29*, 125.
(49) Novak, F. P.; Balasamugan, K.; Vishawanadham, K.; Parker, C. D.; Wilk, Z. A.; Mattern, D.; Hercules, D. M. *Int. J. Mass Spectrom. Ion Phys*. **1983**, *53*, 135.
(50) Cooks, R. G.; Lauritsen, F. R.; Kotiaho, T.; Bauer, S. J.; Choudhry, T. K.; Dejarme, L. E. *Proceedings of the 40th ASMS Conference on Mass Spectrometry and Allied Topics* May 1992, Washington, DC; p 497.

WI), revealed ~70% absorbance at 10.6 μm. Therefore, it is possible to heat the vacuum side of the membrane by irradiating it with a CO_2 laser and induce semivolatile permeate molecules to rapidly desorb intact from the surface. Under laser irradiation conditions, the rate of desorption will increase; therefore, C_2 will decrease (ideally, $C_2 = 0$). The direct membrane heating will also increase the diffusion coefficient, D, of the analyte. LD−MIMS will, therefore, increase the permeation rate and the performance in terms of sensitivity and response time. The silicone membrane has low thermal conductance; therefore, the absorbed energy diffuses slowly into the bulk of the membrane, causing the local surface temperature to remain higher than that of the bulk. This temperature gradient should further enhance the desorption process. All LD−MIMS mass spectra show a predominant PAH molecular ion, confirming that the main result of laser irradiation is, indeed, evaporation. In addition, the mass spectra also consist of a series of background peaks originating from the membrane itself at m/z values 149, 167, 239, 299, 345, 355, 429, and 503. Since the membrane does not evaporate, the peaks seem to correspond to additives like plasticizers and small stable polymer units that are the result of pyrolysis. The exact identity of the ions was not determined. The membrane peaks ultimately limit the sensitivity in the full-scan mode; hence, the selected ion mode (SIM) was preferred for most experiments.

Evidence of Laser Desorption. As discussed previously, the rate of desorption of semivolatile species may be so slow that the permeate molecules actually accumulate on the vacuum side of the membrane surface and form a thin film ($C_2 > 0$). This phenomenon was observed in our studies even at low PAH concentrations. When the silicone membrane that has been exposed to several milliliters of PAH solutions during a typical MIMS experiment is removed from the probe, a thin film of whitish crystals is visible on the vacuum side of the membrane. But when laser heating is applied, the surface molecules desorb, resulting in a "clean" membrane. After one such LD−MIMS experiment, the silicone membrane was photographed using a CCD camera attached to a Zeiss microscope (model Axiovert 100-TV, Zeiss Inc., Thornwood, NY) and is shown in Figure 4B. This membrane was exposed to approximately 300 mL of a 50 ppb each mixture of naphthalene, anthracene, and pyrene and irradiated multiple times with a low-powered (<1 W) CO_2 laser under continuous conditions (~90 min total irradiation). Figure 4A shows a schematic identifying the various regions of the circular membrane, their approximate dimensions, and the region that was photographed using the microscope. In our probe design, as described previously, region 1 is sandwiched (hidden) between a Teflon O-ring spacer and a stainless steel cap. It is therefore not exposed to sample or to the laser. Only the circular region 2 (diameter 0.2 in.) is exposed to both the sample on the solution (high-pressure) side and laser on the vacuum (low-pressure) side. Even though the beam dimensions cover the entire region 2, the effective area over which laser desorption occurs appears to be smaller (region 3) in practice. This could be due to the fact that, in a Gaussian CO_2 laser beam, the power density (energy) is maximum in the beam center and decreases toward the periphery. Thus, the probability of desorption also decreases away from the beam center, and a ringlike area due to incomplete desorption remains. Using low resolution, a small portion of the membrane

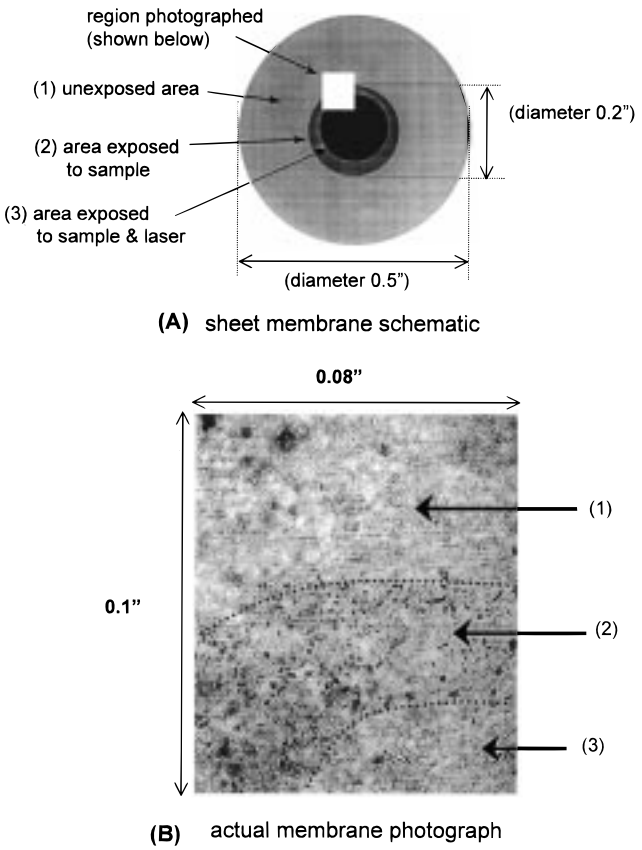

Figure 4. Photograph of a small portion of the silicone membrane after a typical LD−MIMS experiment. The photograph is reproduced in part B, and a schematic explaining the different regions (areas) is shown in part A. Area 1 is hidden (not exposed) from the sample and the laser. The areas marked 2 and 3 have been exposed to the sample and the laser. Area 2 shows that the analyte molecules have crystallized on the membrane surface, whereas area 3 is where laser desorption has occurred, and no crystals are visible, i.e., the surface is clean.

(~0.1 in. × 0.08 in.) was photographed and is reproduced in Figure 4B. The three regions defined in Figure 4A are emphasized using dotted lines in the photograph for comparison. Since region 1 was not exposed to the sample or the laser, it is "clean". Regions 2 and 3 were both exposed to the sample mixture and laser, but analyte crystals can be only be seen scattered in region 2, while region 3 appears relatively clean. This is due to the laser desorption process, which prevents sample molecules from accumulating in region 3. This visibly demonstrates the effect of slow desorption of the PAHs and the capability of the laser to assist in the desorption of these surface-bound molecules.

Laser Desorption Using an External Interface. Laser desorption was first attempted using the external interface (Figure 2) as this requires only minor instrument modifications and simplifies laser alignment. As previously described, in this configuration the DIMP fits into the Cajon chamber, and the laser is fired from the opposite end through the KRS-5 salt window onto the membrane. The inside of the interface is continuously flushed with helium gas to transport the permeate/desorbate to the ion source of the GCQ. Data shown in Figures 5−9 were obtained in this configuration.

Figure 5 shows the selected ion chromatograms of naphthalene (MW 128, bp 218 °C), anthracene (MW 178, bp 340 °C), and

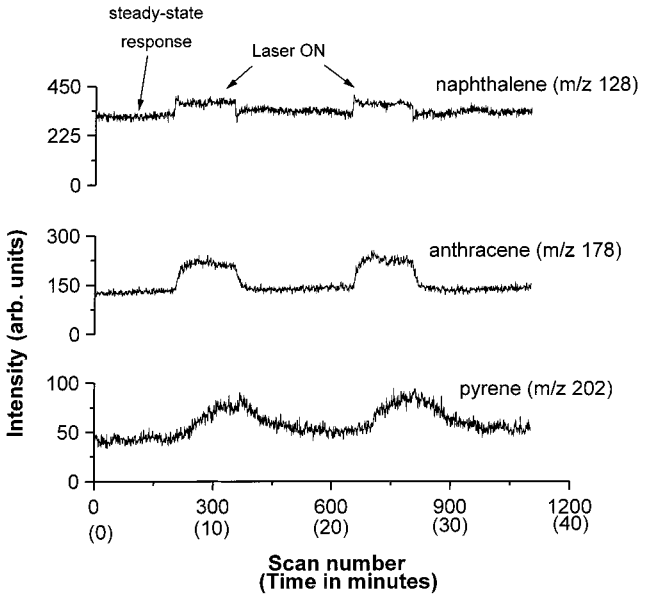

Figure 5. Selected (extracted) ion chromatogram showing the steady-state signals for naphthalene (*m*/*z* 128), anthracene (*m*/*z* 178), and pyrene (*m*/*z* 202). The peaks show the increase in the signal as a result of laser irradiation.

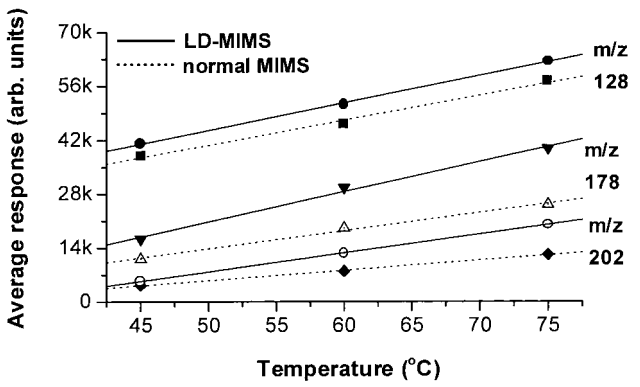

Figure 6. Average response for naphthalene (*m*/*z* 128), anthracene (*m*/*z* 178), and pyrene (*m*/*z* 202) under normal and laser desorption MIMS conditions, plotted versus temperature. The signal increases linearly with temperature under both conditions, but the rate of increase with temperature, given by the slope of the lines, is greater when laser desorption is employed.

pyrene (MW 202, bp 393 °C). These were obtained by analyzing an aqueous mixture containing 4 ppb each of naphthalene, anthracene, and pyrene. A steady baseline was obtained with pure water prior to continuous sample introduction. Once the signal for each compound reached equilibrium (in approximately 60 min at 2 mL/min), the membrane was irradiated with a continuous low-powered (0.5 W) laser beam twice for 5 min each. Two identical laser desorption peaks over the steady-state baseline were obtained for each compound, as shown in Figure 5. For comparing the responses with and without laser desorption for the three compounds, the areas under each peak were background subtracted, averaged, and normalized. The steady-state signal obtained under normal MIMS conditions, i.e., without laser irradiation, is referred to as the background, and the area under the same number of scans, immediately adjacent to each laser desorption peak, is used for subtraction. Thus, the increase in response over the normal MIMS response is obtained as a percentage, allowing comparison between the three compounds.

The steady-state permeation rate and, hence, the signal intensity are governed by the concentration gradient and the diffusion coefficient, *D*. As explained previously, the permeation rate of semivolatile PAHs is affected by their lower desorption rate. Accordingly, the signal intensity for the relatively smaller (large *D*) and more volatile (high desorption rate) naphthalene is the highest (310 ± 11 counts), followed by the relatively larger (small *D*) and less volatile (low desorption rate) anthracene (127 ± 6 counts) and pyrene (42 ± 4 counts). Here we assume that equal fractions of naphthalene, anthracene, and pyrene are absorbed in the membrane at the solution side and that the absorption process is not affected by laser irradiation. The coupling effects, wherein the absorption and diffusion of one compound is influenced by the other compounds of the mixture, are also neglected. When the membrane, under steady-state conditions, is irradiated with the laser, the permeation rate and, hence, the signal intensity increase and reach a higher steady-state level. The rate of desorption no longer is a limiting factor; therefore, the steady-state intensity will be dependent only on the diffusion coefficient, *D*, under the LD−MIMS conditions. *D* will also determine the response time, which will be the shortest for naphthalene (signal reaches steady state rapidly) because it has the largest diffusion coefficient (smallest molecular size), while it will be the longest for pyrene due to its largest size and, hence, smallest *D*. In terms of percent increase, naphthalene shows the smallest increase (∼10%), followed by anthracene (57%) and pyrene (64%). This indicates that the increase in response is inversely related to the sample volatility. In general, LD−MIMS will be least effective for (volatile) compounds, like naphthalene, that permeate efficiently under normal MIMS membrane conditions. The normal and LD−MIMS responses could also be affected by desorbate/permeate molecules condensing (adsorbing) on the inner walls of the interface chamber or the transfer line tubing after they have left the membrane surface and are en route to the ion source. This would further extend the response times (broaden the peaks) and likely lower the sensitivity. Permeate condensation and, hence, degradation in performance will be most severe for pyrene and will least affect naphthalene. The internal interface was designed to avoid this problem as discussed later.

The influence of probe (solution) temperature on the laser desorption response was investigated under steady-state conditions. In this study, the above experiment was performed at three different probe temperatures (45, 60, and 75 °C) using the same naphthalene/anthracene/pyrene mixture. This is the conventional method of heating described previously wherein the membrane temperature is controlled by the heated solution. Ion chromatograms similar to those shown in Figure 5 showing the laser desorption peaks were obtained. The averaged background-subtracted peak areas are plotted versus temperature in Figure 6. The results indicate that, as the temperature increases, the normal steady-state signal as well as the LD−MIMS signal increases almost linearly for all three compounds. This is expected because increasing the solution (membrane) temperature increases the diffusion coefficient and, hence, the permeation rate (*F*). However, the solution temperature is not sufficient for rapid desorption, which therefore damps the increase in *F*. But

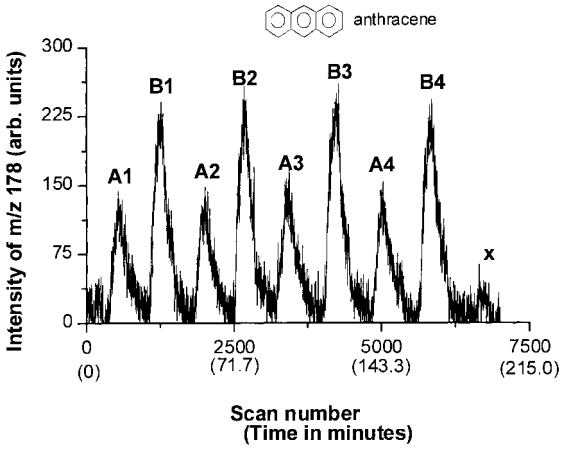

Figure 7. Selected ion chromatogram for *m*/*z* 178 obtained by injecting multiple aliquots of a 25 ppb solution of anthracene using flow injection. During alternate injections, the membrane was simultaneously irradiated by the laser to yield peaks B1−B4. The normal MIMS response is represented by peaks A1−A4. The peak marked X is the laser desorption response to a blank (background water).

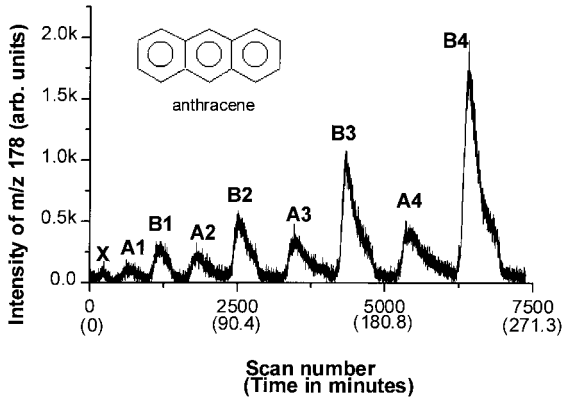

Figure 8. Selected ion chromatogram for *m*/*z* 178 obtained by sequentially injecting 10, 25, 50, and 100 ppb solutions of anthracene using flow injection. Each solution was injected twice, but the membrane was simultaneously irradiated with the laser during the second injection. Peaks A1−A4 represent the normal MIMS response (without laser irradiation), while peaks B1−B4 represent the response with laser irradiation for the 10, 25, 50, and 100 ppb solutions, respectively. The peak marked X is the blank.

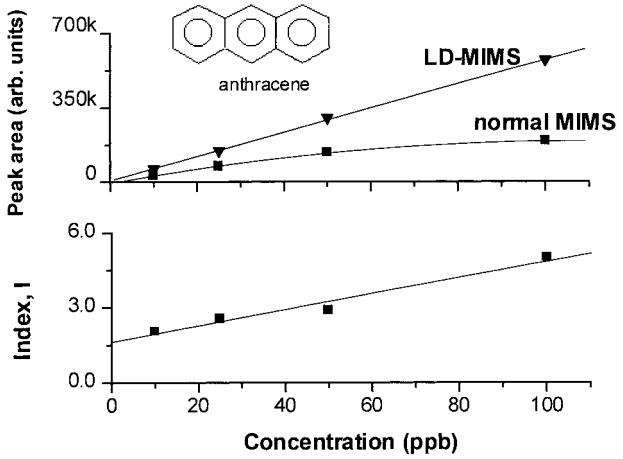

Figure 9. Peak areas and index, *I*, for the data shown in Figure 8, plotted versus concentration. The higher peak areas obtained with LD−MIMS reflects the gain in sensitivity. The index plot reflects the combined improvements in both the sensitivity and response time obtained by laser desorption.

when laser desorption is employed, the rate of desorption is no longer a limiting factor, and hence the rate of increase is faster (as given by the slopes of the lines). The improvement in performance is inversely related to the volatility of the sample. Hence, naphthalene shows the smallest percent increase (8.7% at 45 °C to 10% at 75 °C), while pyrene shows the biggest increase (24.7% at 45 °C to 63.9% at 75 °C) in response over the normal MIMS response. We can also conclude from these results that high (75 versus 45 °C) solution temperature yields better LD−MIMS performance, despite the fact that analyte solubility in the membrane decreases with increasing temperature. In a LD−MIMS analysis of species having low diffusion coefficients, the need for increased mobility (diffusion) is thus more critical than the need for higher solubility.

In the above experiments, data were acquired under steady-state conditions, which provides the maximum sensitivity in MIMS. However, it is seldom employed routinely since it is time-consuming and requires large sample volumes, especially for samples with low diffusion coefficients, like PAHs. The flow injection (FI) technique, in which only small sample volumes (plugs) are injected into a continuously flowing background solution, is therefore commonly employed. This minimizes sample consumption and is simple and highly reproducible. In addition, the segmented nature of sample introduction also allows for faster sampling. In FI-MIMS, there is no need to reach steady-state since FI peak areas are proportional to the analyte concentration and, hence, can be used for quantitation.[17] Figures 7−9 show the data obtained using FI sample introduction in the external laser desorption configuration.

In one such experiment, multiple 10-mL (flow rate 2 mL/min) injections of a 25 ppb aqueous solution of anthracene (MW 178) were analyzed under normal and LD−MIMS conditions. The results are shown in the ion chromatogram in Figure 7. Peaks A1−A4 indicate the normal MIMS response, while B1−B4 were obtained with simultaneous laser heating. Laser irradiation was continuous (0.5 W) and initiated the moment the sample plug reached the membrane. It was terminated when the signal approached baseline (total irradiation ~10 min/peak). This was repeated for alternate injections to get the peaks B1−B4. The peak marked X is the blank which was obtained under identical laser heating conditions but in the absence of the sample for use in background subtraction. In FI-MIMS analysis, the analyte concentration in the solution is changing with time as is the permeation rate and, hence, the response. Initially, the concentration increases with time, resulting in an increase in the signal. Once the sample plug passes across the membrane, the concentration gradient decreases, and the signal falls. Note that steady state is not reached in FI; hence, the signal takes the shape of narrow peaks, as seen in the ion chromatogram. The peak area is determined by the analyte concentration in the solution or, more correctly, the concentration gradient and the analyte diffusion coefficient. The results show that the MIMS response is increased and still reproducible when laser irradiation is employed. On average, the laser desorption peak area is 2 times greater than the area of the peak from a normal FI-MIMS response. The relative standard deviation (RSD) for the background-subtracted

peak areas is 6.5% and 2.2% for peaks A1−A4 and B1−B4, respectively.

In another experiment, the linearity of LD−MIMS was tested for a series of anthracene samples having concentrations of 10, 25, 50, and 100 ppb in water. The selected ion chromatogram (m/z 178) was recorded by sequentially injecting samples of increasing concentration using the FI method. Each sample was injected twice back-to-back; however, during the second injection, the membrane was simultaneously irradiated with a 0.5-W continuous laser beam. The selected ion chromatogram (Figure 8) shows the alternating peaks obtained under normal (peaks A1−A4) and LD−MIMS (peaks B1−B4) conditions at 10, 25, 50, and 100 ppb concentrations, respectively. A blank, i.e., LD−MIMS response in the absence of sample, was also recorded (peak X). The background-subtracted peak areas for each sample are plotted versus concentration in Figure 9. The normal MIMS response best fits to a nonlinear second-order polynomial with $R^2 = 1.0$ and the LD−MIMS response to a straight line ($R = 0.9997$).

As discussed previously, the linearity between F and analyte concentration under normal MIMS conditions is affected by the slow desorption process, especially at higher concentrations. The response (signal intensity) is determined by the amount and rate of desorption of the permeate molecules from the surface. When the number of molecules desorbing from the surface reaches a maximum value (surface saturation), the permeation rate (response) will become constant and not increase even when the solution concentration increases. The rate of desorption, therefore, limits the dynamic range at the higher concentration. In the case of LD−MIMS, the desorption is continuous and efficient even when the concentration (number of molecules on the surface) increases. Therefore, the concentration gradient is maintained, and the permeation rate changes linearly with concentration. Laser desorption, therefore, improves the dynamic range linearity of MIMS. The upper end of the dynamic range will eventually become nonlinear when the analyte solubility in the membrane does not increase proportionally to its concentration in the solution. This phenomenon is not a factor within the concentration range of this experiment, as indicated by the linearity of the LD−MIMS response, but will ultimately limit the dynamic range as in any MIMS experiment.

The FI peak shape (height and response time) provides important information about the permeation process. Under normal MIMS conditions, the slopes of the rising edge (rise time) and the falling edge of the peak (fall time) are governed by both the diffusion coefficient, D, of the compound and its desorption rate. The longer the residence time, i.e., the time spent by the molecules in the membrane (given by D) and on the surface (given by the desorption rate), the longer will be the response time. Since LD−MIMS increases the desorption rate and D, both the flux magnitude (peak area) and the residence (response) time are better than those obtained under normal MIMS conditions. To make this comparison, we define a dimensionless parameter called the improvement index (I) as

$$I = \frac{\left\{\dfrac{\text{peak area (arb units)}}{\text{peak rise + fall time (min)}}\right\}_{\text{under LD−MIMS conditions}}}{\left\{\dfrac{\text{peak area (arb units)}}{\text{peak rise + fall time (min)}}\right\}_{\text{under normal MIMS conditions}}}$$

where the peak rise and fall times are calculated as the time it takes in minutes for the signal to rise from 10% to 90% ($t_{10-90\%}$) and fall from 90% to 10% ($t_{90-10\%}$) of its maximum value, respectively. The index, I, is plotted versus concentration in Figure 9 and fit to a straight line ($R = 0.9927$). The response time reflects the time the molecules spend in the membrane (including the surface), i.e., the residence time, while the ratio of peak area/response time (counts/min) reflects the overall efficiency with which the analyte molecules are transported across the membrane. The value of the index, I, is thus the factor by which transport efficiency increases if laser desorption is employed. Note that high transport efficiencies allow for higher sampling frequency. The index, I, increases with concentrations as the normal MIMS response becomes nonlinear.

Laser Desorption Using an Internal Interface. With the external interface, it was suspected that sample condensation (adsorption) within the interface and tubing was affecting the performance. Therefore, an internal interface was designed to perform laser desorption within the mass spectrometer vacuum system. It is also common knowledge in MIMS that better performance is achieved when the membrane is located close to the ion source as opposed to some distance away for reasons mentioned before.[18,25] In the internal LD−MIMS configuration (Figures 1 and 3), the membrane forms one wall of the ion source, and the laser beam is incident normal to the membrane plane. The desorbate plume expands directly into the ion source cavity, where it is bombarded by electrons from the orthogonal EI filament.

In comparison to the external interface, LD−MIMS of naphthalene, anthracene, and pyrene in the internal interface showed little or no improvement in performance over normal MIMS. Under normal MIMS conditions, the membrane temperature, which determines the efficiency of pervaporation, is about 80 °C in the external interface, while it is close to 125 °C (the source temperature) in the internal interface due to its proximity to the ion source. Therefore, in the internal configuration, with the vacuum side of the membrane surface exposed to the heat radiated by the hot ion source, the desorption of these compounds is sufficiently rapid even under normal MIMS conditions compared to that in the external interface. This result again confirms that laser desorption is least effective when the permeation rate is rapid under normal MIMS conditions. This was not the case when higher PAHs such as chrysene (MW 228, bp 448 °C), benzo[*b*]-fluoranthene (MW 252, bp 480 °C), and indeno[123-*cd*]pyrene (MW 276, bp 530 °C) were analyzed in the internal interface, as discussed below. Note that these compounds yielded poor results (low sensitivity and long response times) using the extrernal interface.

The effect of laser irradiation on the steady-state signal of benzo[*b*]fluoranthene and indeno[123-*cd*]pyrene was studied. This experiment is analogous to that described in Figure 5. A mixture containing 10 ppb of each compound was continuously injected into the DIMP. After about 60 min at 2 mL/min, the molecular ion signal for both compounds stabilized. The CO_2 laser was then fired for a period of 2 min each at three different time intervals using the pulsed irradiation mode, wherein a 2-W continuous beam was gated (pulsed) using the Uniblitz mechanical shutter. The timing of the shutter opening and width was synchronized with

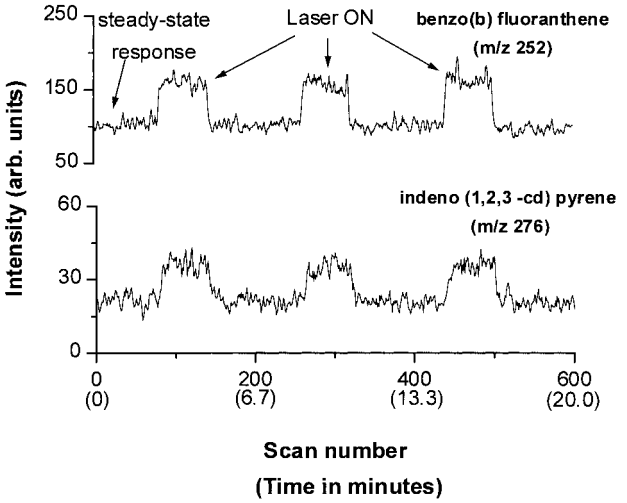

Figure 10. Selected ion chromatogram showing the steady-state signals for benzo[*b*]fluoranthene (*m*/*z* 252) and indeno[123-*cd*]pyrene (*m*/*z* 276). The membrane was irradiated for three separate instances to produce the three identical peaks shown in the figure.

the start of the ionization period and its duration in the GCQ scan. The response obtained is shown as selected ion chromatograms in Figure 10. As with the previous steady-state experiment (Figure 5), identical peaks were obtained for each instance of laser irradiation. The areas under each peak were background subtracted, averaged, and normalized. For background subtraction, the area under the normal steady-state signal (same number of scans) immediately adjacent to each laser desorption peak was used. Values of 45% and 58% were obtained for benzo[*b*]-fluoranthene and indeno[123-*cd*]pyrene, respectively. The values represent the percent increase in response over the normal MIMS response, and, as expected, the value for the relatively less volatile indeno[123-*cd*]pyrene is higher. Also note that the peak rise and fall times obtained in this configuration are much smaller as compared to those obtained in the external configuration (Figure 5). This may be due to the fact that sample condensation does affect the performance in the external interface but not in the internal configuration.

In another experiment, multiple 10-mL plugs of a 10 ppb solution of benzo[*b*]fluoranthene were injected at 2 mL/min flow rate using the FI method. Alternate injections were irradiated in the pulsed mode described above. The results obtained are shown in Figure 11. Peaks B1−B4 were obtained with and peaks A1−A4 without laser irradiation. The results show the excellent reproducibility obtained with both normal MIMS (RSD = 4.3%) and LD−MIMS (RSD = 1.0%). The LD−MIMS peak areas are 2.2 times that of normal MIMS.

A series of samples of indeno[123-*cd*]pyrene of varying concentration were analyzed under identical conditions with and without laser irradiation in an experiment analogous to that described in Figure 8. Ten-milliliter samples of 25, 50, 100, and 250 ppb were injected sequentially using the FI method in both trials. The LD−MIMS data were recorded using pulsed laser irradiation conditions similar to those mentioned above for benzo-[*b*]fluoranthene. The results from this experiment are shown in Figure 12. The background-subtracted peak areas for normal MIMS best fit to a quadratic curve (R^2 = 0.9993), and the LD−MIMS data points best fit to a straight line (R = 0.9991). The

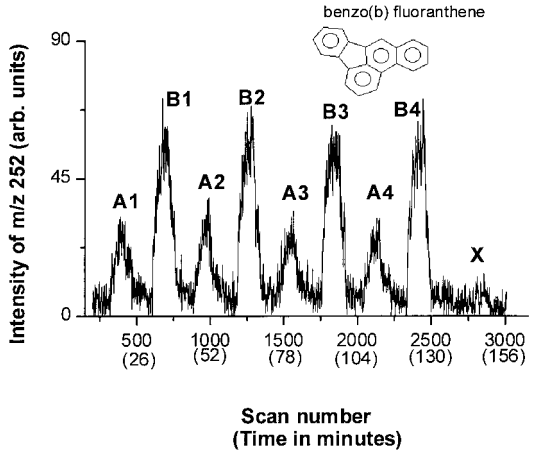

Figure 11. Selected ion chromatogram for *m*/*z* 252 obtained by injecting multiple aliquots of a 10 ppb solution of benzo[*b*]fluoranthene using flow injection. Peaks B1−B4 were obtained with simultaneous laser irradiation, while peaks A1−A4 represent the MIMS response without laser irradiation. Peak X is the blank.

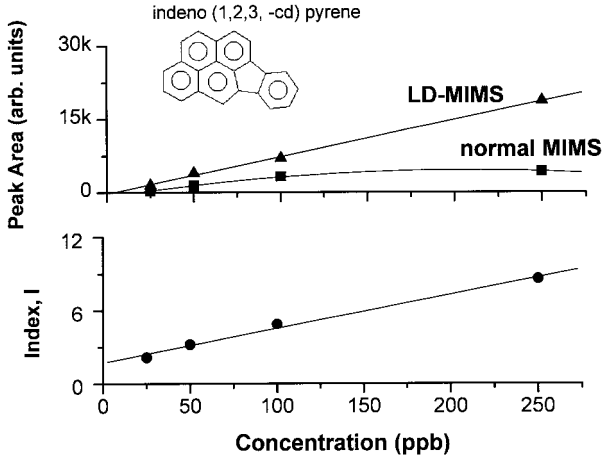

Figure 12. Results from an experiment in which 25, 50, 100, and 250 ppb solutions of indeno[123-*cd*]pyrene (*m*/*z* 276) were analyzed with and without laser irradiation. The peak areas and index, *I*, increase with concentration.

response becomes nonlinear as concentration increases under normal MIMS conditions but remains linear when laser desorption is employed. In terms of percent increase over normal MIMS, the improvement is better when higher concentrations are analyzed with LD−MIMS. This behavior is similar to that of anthracene (Figure 9) discussed above. The improvement index, *I*, versus concentration plot, also shown in Figure 12, is fit to a straight line (R = 0.9955) and shows a linear increase with concentration. This result is in agreement with previous results, which indicate that the improvement in performance (both sensitivity and response time) due to laser heating is inversely related to the volatility of the sample.

CONCLUSIONS

This paper reports the first demonstration of laser desorption−membrane introduction mass spectrometry. We have shown how the silicone membrane can be directly heated using a low-powered CO_2 laser beam to rapidly desorb intact permeate molecules from the membrane surface. The direct membrane heating also increases the diffusion coefficient, *D*. This increases the perme-

ation rate and, hence, the MIMS response. Overall, the greater pervaporation efficiency obtained using LD−MIMS improves both sensitivity and response times when analyzing semivolatile compounds. We have demonstrated this by analyzing high boiling point (200−530 °C) PAHs directly from water without any pretreatment using MIMS. Some important characteristics of LD−MIMS are that (i) the amount of heat energy deposited in the membrane is higher than that possible with conventional MIMS techniques, (ii) heat is applied only when needed, i.e., during sample introduction, (iii) heat is localized only at the surface where it is needed i.e., the vacuum side of the membrane, and (iv) desorption is rapid and nonselective. This method is universal in that it can be applied to enhance the MIMS performance of any species that is large in size and/or has low volatility. LD−MIMS performance might be further enhanced if microporous membranes, which provide higher analyte fluxes, are used. Other types of membranes, including the newer liquid membranes[26] which are easily chemically modified to make them more selective toward target compounds, could also be utilized with LD−MIMS. The method is suitable for use in conjunction with tandem mass spectrometry and ion−molecule reaction methods to resolve complex mixtures and isomeric ions.[51−53] The sample introduction and laser irradiation steps were simultaneous in the experiments described here. But they can also be performed sequentially in a manner similar to the trap-and-release method described by Lauritsen et al.[28,29] In such an analysis, the membrane would be first exposed to the sample for several minutes at low solution temperatures to get better absorption efficiency and then irradiated by the laser beam for a relatively shorter period to desorb the analyte. The performance of this method in terms of sensitivity and response times has yet to be evaluated. We are currently investigating LD−MIMS using a UV laser. In contrast to IR radiation, the dynamics of heating and desorption are different since the analytes (PAHs) are UV absorbing while the membrane is not. This will extend the life of the membrane and provide selectivity and greater sensitivity by eliminating background ions arising from membrane decomposition. UV laser irradiation also has the potential of directly ionizing permeate molecules, which will eliminate the need for EI postionization and also reduce background ions.

(51) Nourse, B. D.; Cox, K. A.; Morand, K. L.; Cooks, R. G. *J. Am. Chem. Soc.* **1992**, *114*, 2010.
(52) Brodbelt, J. S. *Mass Spectrom. Rev.* **1997**, *16*, 91.
(53) Mosi, A. A.; Cullen, W. R.; Eigendorf, G. K. *J. Mass Spectrom.* **1998**, *33*, 250.

ACKNOWLEDGMENT

We thank Scott Quarmby and Eric Johnson of Finnigan Corp., Austin, TX, for providing and assisting with the beta version of Custom Tune software for the GCQ, Mohan Natesan and the Colton group for allowing use of their Zeiss microscope, and Dr. R. G. Cooks for helpful comments and suggestions. This project was financially supported by the Office of Naval Research under Contract No. N00014-96-WX20426.

Received for review April 20, 1998. Accepted June 1, 1998.

AC980436L